Available online at www.sciencedirect.com
ScienceDirect
Journal of Solid State Chemistry 179 (2006) 3277–3285
JOURNAL OF SOLID STATE CHEMISTRY
www.elsevier.com/locate/jssc

Structural phase transitions in BaV_6O_{11}

Karen Friese[a,*], Yasushi Kanke[b]

[a]Departamento Física Materia Condensada, Facultad de Ciencia y Tecnología, Universidad del País Vasco, Apdo. 644, 48080 Bilbao, Spain
[b]Advanced Materials Laboratory, National Institute for Materials Science, 1-1 Namiki, Tsukuba, Ibaraki 305-0044, Japan

Received 20 December 2005; received in revised form 27 March 2006; accepted 8 April 2006
Available online 29 June 2006

Abstract

BaV_6O_{11} was synthesized under high pressures and crystallizes in a structure closely related to magnetoplumbite. $[V(1)O_6]$-octahedra share common edges and form a Kagomé lattice normal to the hexagonal [0 0 1] direction. The layers are connected in the direction of c via trigonal $[V(3)O_5]$-bipyramids and $[V(2)O_6]$-octahedra, which share common faces. The Ba-atoms are incorporated into cavities of the vanadium oxide framework and are coordinated by 12 oxygen atoms in the shape of a dodecahedron.

Three magnetic anomalies at approximately 250, 115 and 75 K were detected in this compound. All of them are accompanied by anomalies in the specific heat measurement. To characterize possible structural transitions and determine the response of the structure to the magnetic anomalies, single crystal X-ray diffraction studies were carried out in the temperature range from 293 to 80 K. At 250 K the compound undergoes a structural phase transition. The space group above the transition temperature is $P6_3/mmc$, at lower temperature the symmetry reduces to $P6_3mc$. For the refinements in $P6_3mc$ an inversion twin model was used, this way accounting for the loss of the center of symmetry. The structural phase transition is characterized by a small displacement of the V(1)-atom (forming the Kagomé lattice) out of its central position in the octahedra. As a consequence part of the octahedral edges/angles are increased, while the opposite ones are decreased. One limiting surface of the octahedral sheet is corrugated, while the other one is smoothened with respect to the high-temperature structure. This deformation of the octahedral sheets leads to the corresponding geometrical changes in the other coordination polyhedra.

The structural response to the magnetic anomaly at 115 K is weak and mainly observable in the geometric parameters concerning the $[V(1)O_6]$-octahedra and $[V(3)O_5]$-bipyramids. This may serve as a first indication that the corresponding central atoms play an important role in the mechanism of the magnetic phase transition.

Keywords: Magnetoplumbite; BaV_6O_{11}; Structural phase transition; Inversion twin; Single crystal diffraction; Magnetic anomaly; Kagomé lattice

1. Introduction

Compounds with general composition AV_6O_{11} (A = Na, K, Sr, Pb) [1–4] are of special interest due to their magnetic and electric properties [5–23]. Isostructural $SrCo_6O_{11}$ [24], $BaMRu_5O_{11}$ (M = Li, Cu) and $BaM'_2Ru_4O_{11}$ (M' = Mn, Fe, Co) [25] are reported. The compounds crystallize hexagonal, the structures being closely related to the magnetoplumbite structure. The O-anions and A-cations are arranged in a hexagonal close-packing. Two vanadium atoms are coordinated octahedrally by oxygen, while the third is incorporated into a trigonal bipyramidal cavity.

Apart from magnetic phase transitions, these compounds show at least one structural phase transition at the following temperatures, in which the symmetry is reduced from $P6_3/mmc$ to $P6_3mc$:

NaV_6O_{11}	242.7 K	[8,14,20]
KV_6O_{11}	190 K	[4]
SrV_6O_{11}	320 K	[15,20]
PbV_6O_{11}	560 K	[20,21]

*Corresponding author. Fax: +34 94 601 5481.
E-mail address: karen.friese@ehu.es (K. Friese).

0022-4596/$ - see front matter © 2006 Elsevier Inc. All rights reserved.
doi:10.1016/j.jssc.2006.04.059

We report on a new member of the family, BaV_6O_{11}, which was successfully synthesized under high pressure. Specific heat and magnetic susceptibility measurements indicated the presence of structural and magnetic phase transitions in this compound. The aim of this work was to characterize both the room and low-temperature structure of BaV_6O_{11} down to temperatures of 80 K.

2. Experimental

High-pressure synthesis of BaV_6O_{11} was realized analogous to the procedure described in [4] at pressures of 5.5–6.0 GPa and temperatures of 1473–2323 K, using $Ba_2V_2O_7$ and V_2O_3 as starting materials.

Specific heat measurements (see Fig. 1) were carried out with a physical property measurement system from quantum design in the temperature range from 290 to 1.8 K. The magnetic data (see Fig. 2) were collected with a magnetic property measurement system from quantum design in the temperature range from 330 to 5 K. For the measurements in the paramagnetic region a crushed single crystal (0.02518 g) was used; the external magnetic field was 1000 Oe. Measurements in the magnetically ordered region were carried out on a single crystal (0.00053 g) with an external magnetic field parallel to [0 0 1] (2000 Oe, Zero field cool).

Both the specific heat and the magnetic measurements show three anomalies corresponding to temperatures of approximately 250, 115, and 75 K.

Diffraction intensities of a suitable single crystal were recorded with different diffractometers: PW1100 (Philips; 293 and 169 K), Cad4 (Enraf Nonius; 120 and 90 K), IPDS I (Stoe & CIE; 260, 230, 200, 140, 105, and 80 K) and an IPDS II (Stoe & CIE; at the "Single Crystal Diffraction" Beamline of the Institute for Synchrotron radiation, Anka, Forschungszentrum Karlsruhe, Germany; 100 K). For cooling N_2 cryostats from Oxford Cryosystems and Oxford Instruments were employed.[1]

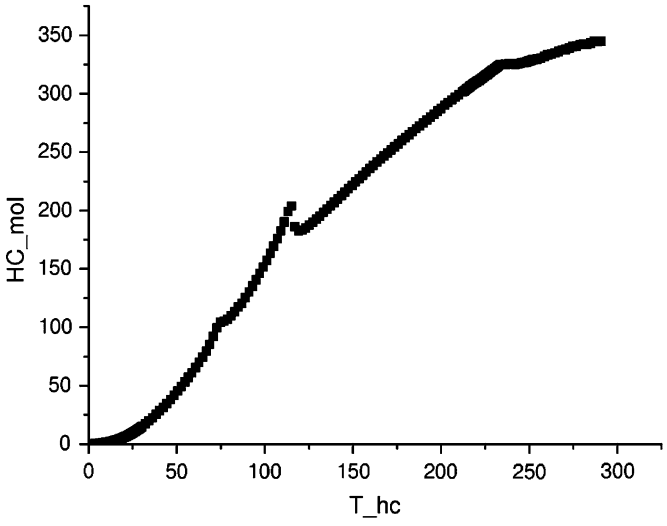

Fig. 1. Specific heat measurement of BaV_6O_{11}. Data are given in Joule per Kelvin per mole.

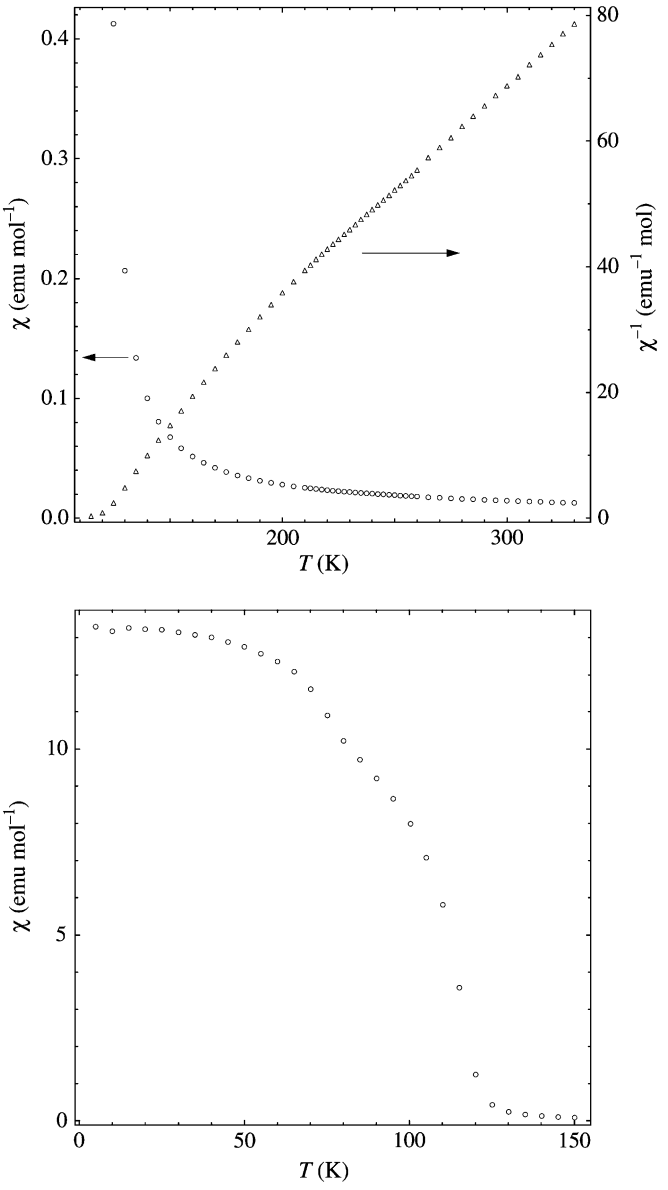

Fig. 2. Magnetic susceptibility and inverse magnetic susceptibility versus temperature of BaV_6O_{11}. The external magnetic field in the paramagnetic region was 1000 Oe. Measurements in the magnetically ordered region were carried out with an external magnetic field parallel to [0 0 1] (2000 Oe, Zero field cool).

Lattice parameters were obtained from the same single crystal using the Gandolfi method on an IPDS II (Stoe & CIE) at the beamline "Single Crystal Diffraction" at the Institute for Synchrotron Radiation, Anka, Forschungszentrum Karlsruhe, Germany. The obtained two dimensional images were integrated with the software X-Area [26] and the lattice parameters were refined employing the

[1]Further experimental and structure determination details of the crystallographic investigations can be obtained from the Fachinformationszentrum Karlsruhe, D-76344 Eggenstein-Leopoldshafen, Germany, on quoting the depository numbers CSD 416450–416460.

LeBail method with the program Jana2000 [27]. Lattice parameters for the single crystal investigations were interpolated from these data.

3. Structure solution and refinement

The structure at room temperature was solved via direct methods with the program Sir97 [28]. For the other temperatures the starting coordinates were deduced from the room temperature model. All structure refinements were carried out with the program Jana2000 [27].

The diffraction patterns could be indexed with hexagonal metrics and the internal R-values indicated hexagonal symmetry. The systematic absences $hh2\bar{h}l : l = 2n + 1$ yielded the space groups $P6_3/mmc$, $P6_3mc$ and $P\bar{6}2c$ as possible choices. All options were tried for the refinement of the data set at room temperature. As results in the acentric space groups did not lead to significantly better agreement factors, we considered the space group $P6_3/mmc$ to be the correct choice. This space group was also confirmed for the data set at a temperature of 260 K.

At approximately 250 K a structural phase transition is suggested by specific heat measurements (see Fig. 1). Its existence was confirmed by the fact that the data sets at 230 K and lower temperatures show significantly better agreement factors in space group $P6_3mc$ than in the corresponding centrosymmetric supergroup. Trial refinements in the remaining maximal subgroups of $P6_3/mmc$, which are in accordance with the observed extinction rule, namely $P\bar{6}2c$, $P\bar{3}1c$, and $Cmcm$ did not lead to better results for any of the temperatures below 250 K and we are therefore confident that $P6_3mc$ is the correct choice for all the investigated temperatures below 250 K. In all refinements in space group $P6_3mc$ an inversion twin model was assumed, this way accounting for the loss of the center of symmetry in the phase transition. Further refinement details are given in Table 1.

The datasets at the individual temperatures were measured up to different resolution limits. At 293 and 169 K our interest was centered on a reliable structure determination of the two different modifications and we measured up to the necessary θ range to achieve this aim. Around 115 K the magnetic susceptibility measurements indicated a magnetic anomaly. Therefore, the measurements at 120 and 90 K were carried out up to the highest θ angles where diffracted intensities could still be recorded as we assumed that datasets of very high quality were indispensable to detect any existing structural response to the magnetic changes. Datasets at the remaining temperatures (260, 230, 200, 140, 105, 100 and 80 K) were mainly recorded to obtain additional information about the temperature dependence of structural parameters and were measured up to a limited θ range. Accordingly, the information content about the displacement parameters of the atoms for these last temperatures is also limited and we encountered problems in refining the corresponding parameters, as they showed a tendency to assume negative values. To overcome these problems, we fixed the corresponding parameter (u_{11}, u_{22} or u_{33}) to a value of 0.005, which we extrapolated on the basis of the refined values at the other temperatures.

Final atomic coordinates and isotropic displacement parameters for selected temperatures (293, 169, 120 and 90 K) are listed in Table 2. Interatomic distances are listed in Table 3.

4. Discussion

At room temperature BaV_6O_{11} crystallizes hexagonal, space group $P6_3/mmc$. The structure is isotypical to the corresponding structures of NaV_6O_{11} [1,7], KV_6O_{11} [4], SrV_6O_{11} [2,7,15] and PbV_6O_{11} [3,20,21] at the relevant temperatures. In the structure of BaV_6O_{11} the O-anions and Ba-cations are arranged in a hexagonal close-packing. Two vanadium atoms are coordinated octahedrally by oxygen, while the third is incorporated into a trigonal bipyramidal cavity.

Table 1
Refinement details and agreement factors for BaV_6O_{11} at the different temperatures

Temp. (K)	Reflections (obs/all)	Reflections (unique obs/all)	Red.	R_{int} (obs)	R_{int} (all)	R_w (obs)	R_w (all)	R (obs)	R (all)
Space group $P6_3/mmc$									
293	1186/1434	586/653	1.03	0.0096	0.0100	0.0202	0.0249	0.0246	0.0250
260	2998/3661	239/256	13.223	0.0595	0.0598	0.0235	0.0223	0.0286	0.0223
Space group $P6_3mc$									
230	3087/3665	460/488	6.945	0.0622	0.0624	0.0264	0.0281	0.0305	0.0281
200	3140/3660	463/486	6.963	0.0570	0.0572	0.0243	0.0260	0.0289	0.0260
169	1267/1429	1214/1264	1.030	0.0090	0.0090	0.0232	0.0287	0.0256	0.0288
140	3194/3662	467/486	6.967	0.0558	0.0560	0.0241	0.0251	0.0278	0.0251
120	7418/8331	2435/2595	3.047	0.0554	0.0557	0.0397	0.0370	0.0436	0.0370
105	3223/3655	469/486	6.953	0.0628	0.0629	0.0255	0.0258	0.0288	0.0258
100	3765/4021	483/507	7.931	0.1032	0.1035	0.0289	0.0375	0.0435	0.0402
90	7428/8240	2908/3095	2.54	0.0321	0.0325	0.0298	0.0312	0.0335	0.0312
80	3228/3652	469/487	6.932	0.0606	0.0607	0.0260	0.0277	0.0299	0.0277

(Red. = Redundancy).

Table 2
Atomic coordinates and isotropic displacement parameters for BaV_6O_{11} at selected temperatures

Atom	x	y	z	U_{iso}	Temperature
Ba	0.3333	0.6667	0.25	0.00596 (6)	293 K
V1	0.5	0	0	0.00616 (10)	
V2	0	0	0.14576 (4)	0.00468 (9)	
V3	0.3333	0.6667	0.75	0.00789 (14)	
O1	0.17231 (14)	0.3446 (3)	0.07955 (9)	0.0064 (3)	
O2	0.15079 (19)	0.3016 (4)	0.75	0.0069 (5)	
O3	0.3333	0.6667	0.58904 (17)	0.0070 (4)	
Ba	0.3333	0.6667	0.25	0.00389 (6)	169 K
V1	0.49328 (6)	0.98656 (13)	−0.00084 (12)	0.00375 (10)	
V2a	0	0	0.1424 (2)	0.00315 (8)	
V2b	0	0	0.3514 (2)	0.00315 (8)	
V3	0.3333	0.6667	0.73764 (6)	0.0027 (2)	
O1a	0.1723 (2)	0.3446 (5)	0.0784 (3)	0.0046 (3)	
O1b	0.1722 (2)	0.3444 (5)	0.4184 (3)	0.0046 (3)	
O2	0.15095 (18)	0.3019 (4)	0.7481 (4)	0.0061 (5)	
O3a	0.3333	0.6667	0.5856 (5)	0.0077 (5)	
O3b	0.3333	0.6667	0.9050 (5)	0.0077 (5)	
Ba	0.3333	0.6667	0.25	0.00275 (5)	120 K
V1	0.49272 (6)	0.98544 (13)	0.99492 (12)	0.00277 (9)	
V2a	0	0	0.14141 (16)	0.00219 (8)	
V2b	0	0	0.35009 (16)	0.00219 (8)	
V3	0.3333	0.6667	0.73754 (9)	0.00330 (18)	
O1a	0.1723 (3)	0.3447 (6)	0.0773 (3)	0.0035 (3)	
O1b	0.1718 (3)	0.3436 (6)	0.4178 (3)	0.0035 (3)	
O2	0.1512 (2)	0.3024 (5)	0.7452 (3)	0.0037 (5)	
O3a	0.3333	0.6667	0.5805 (3)	0.0034 (5)	
O3b	0.3333	0.6667	0.9002 (4)	0.0034 (5)	
Ba	0.3333	0.6667	0.25	0.00221 (3)	90 K
V1	0.49210 (4)	0.98420 (7)	−0.00559 (5)	0.00230 (5)	
V2a	0	0	0.14099 (7)	0.00194 (5)	
V2b	0	0	0.34982 (7)	0.00194 (5)	
V3	0.3333	0.6667	0.73645 (6)	0.00277 (9)	
O1a	0.17206 (19)	0.3441 (4)	0.07693 (18)	0.00325 (16)	
O1b	0.1719 (2)	0.3438 (4)	0.41764 (18)	0.00325 (16)	
O2	0.15189 (16)	0.3038 (3)	0.74506 (18)	0.0035 (3)	
O3a	0.3333	0.6667	0.5814 (2)	0.0036 (3)	
O3b	0.3333	0.6667	0.9003 (3)	0.0036 (3)	

The $[V(1)O_6]$-octahedra share common edges and form a Kagomé lattice normal to the hexagonal [0 0 1] direction (see Fig. 3). The layers are connected in the direction of c via $[V(2)O_6]$-octahedra, which share common faces, and trigonal $[V(3)O_5]$-bipyramids (see Fig. 4). The Ba-atoms are incorporated into cavities of the vanadium oxide framework and are coordinated by 12 oxygen atoms in the shape of a dodecahedron.

Both specific heat and magnetic measurements indicate three anomalies corresponding to temperatures of approximately 250, 115, and 75 K (see Figs. 1 and 2). The lattice parameters and the overall volume of the unit cell decrease slightly with decreasing temperature (see Fig. 5) and no significant discontinuity of their values is observed in the temperature range studied.

The first of the anomalies at 250 K corresponds to a structural phase transition, where the center of symmetry is lost and the space group symmetry reduces to $P6_3mc$. No further change of symmetry was observed in the studied temperature range and according to the results from the structural investigation the $P6_3mc$ phase remains stable down to 80 K.

The inversion center in the structural phase transition at 250 K is retained as additional twinning operation. The reduction of symmetry leads to a splitting of the Wyckoff positions 4*e*, 12*k* and 4*f*, occupied by the atoms V2, O1 and O3, respectively. Thus, instead of the seven symmetrical equivalent positions of the high-temperature phase, 10 symmetrical independent atoms have to be taken into account in the low-temperature phase.

A comparison of the two phases shows that in the higher-symmetrical phase ($P6_3/mmc$) the V(1) Kagomé lattice consists of one regular triangle. Below 250 K these triangles divide into larger and smaller ones at the same time maintaining their geometrical regularity. This is reflected in the branching of the V(1)–V(1) distances (see Fig. 6). The evolution of these distances is not visibly influenced by the magnetic transition at 115 K.

Table 3
Selected distances and angles for BaV_6O_{11} at the different temperatures

	293 K		169 K	120 K	90 K
Ba–O1	6 × 2.7814 (13)	Ba–O1a	3 × 2.790 (4)	3 × 2.798 (4)	3 × 2.803 (2)
		Ba–O1b	3 × 2.757 (3)	3 × 2.749 (4)	3 × 2.745 (2)
Ba–O2	6 × 2.9000 (16)	Ba–O2	6 × 2.8936 (14)	6 × 2.8887 (17)	3 × 2.8890 (11)
V1–V1	4 × 2.8956	V1–V1	2.77727 (7)	2.7579 (7)	2.7477 (4)
V1–O1	4 × 1.9545 (19)	V1–O1a	2 × 1.920 (4)	2 × 1.938 (5)	3 × 1.937 (3)
		V1–O1b	2 × 1.991 (3)	2 × 1.966 (4)	3 × 1.966 (2)
V1–O3	2 × 2.0479 (13)	V1–O3a	2.080 (4)	2.076 (3)	2.0905 (18)
		V1–O3b	2.031 (4)	2.028 (3)	2.018 (2)
V2–V2	2.7694 (8)	V2a–V2b	2.774 (5)	2.768 (3)	2.7670 (13)
V2–O1	3 × 1.9393 (14)	V2a–O1a	3 × 1.922 (3)	3 × 1.920 (3)	3 × 1.917 (2)
V2–O2	3 × 2.0506 (14)	V2a–O2	3 × 2.062 (4)	3 × 2.044 (4)	3 × 2.051 (2)
		V2b–O1b	3 × 1.939 (3)	3 × 1.937 (4)	3 × 1.939 (2)
		V2b–O2	3 × 2.040 (4)	3 × 2.054 (4)	3 × 2.057 (2)
V3–O2	3 × 1.8311 (19)	V3–O2	3 × 1.8307 (18)	3 × 1.822 (2)	3 × 1.8166 (16)
V3–O3	2 × 2.138 (2)	V3–O3a	2.018 (7)	2.083 (5)	2.055 (3)
		V3–O3b	2.221 (7)	2.158 (5)	2.172 (3)
O1–O1	4 × 2.9936 (15)	O1a–O1a	2 × 2.987 (3)	2 × 2.982 (3)	2 × 2.978 (2)
		O1b–O1b	2 × 2.985 (3)	2 × 2.973 (3)	2 × 2.975 (2)
O1–O1	4 × 2.7976 (15)	O1a–O1a	2 × 2.791 (3)	2 × 2.786 (3)	2 × 2.791 (2)
		O1b–O1b	2 × 2.794 (3)	2 × 2.795 (3)	2 × 2.794 (2)
O1–O1	2 × 2.730 (2)	O1a–O1b	2 × 2.735 (5)	2 × 2.726 (5)	2 × 2.722 (3)
O1–O2	4 × 2.7907 (15)	O1a–O2	2 × 2.779 (5)	2 × 2.757 (5)	2 × 2.759 (3)
		O1b–O2	2 × 2.786 (5)	2 × 2.805 (5)	2 × 2.807 (3)
O1–O3	4 × 2.8989 (11)	O1a–O3a	2 × 2.891 (2)	2 × 2.885 (3)	2 × 2.8856 (15)
		O1b–O3b	2 × 2.895 (2)	2 × 2.894 (3)	2 × 2.8940 (16)
O1–O3	2 × 2.761 (2)	O1a–O3b	2.810 (7)	2.847 (6)	2.841 (4)
		O1b–O3a	2.743 (6)	2.694 (5)	2.703 (3)
O2–O2	2 × 2.6197 (17)	O2–O2	2 × 2.6167 (19)	2 × 2.616 (3)	2 × 2.629 (2)
O2–O3	2 × 2.815 (2)	O2–O3a	2.826 (6)	2.843 (5)	2.827 (3)
		O2–O3b	2.770 (6)	2.746 (5)	2.742 (3)

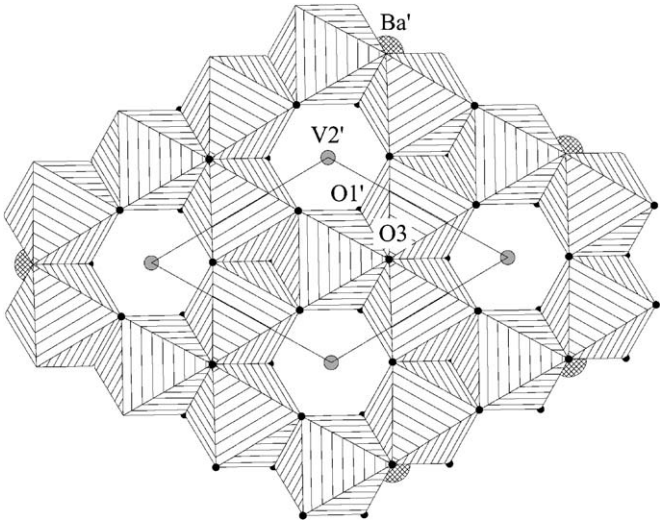

Fig. 3. a,b-Projection of the structure of BaV_6O_{11} at 293 K. Limits of the projection are $0.25<z<0.75$. Octahedra around V(1) are shown. Large hatched circles represent Ba-, small grey circles represent V(2) atoms. Drawn with Atoms [29].

The best way to understand the remaining changes in the structure before and after the transition from $P6_3/mmc$ to $P6_3mc$ is by looking at the octahedral sheet. The limiting

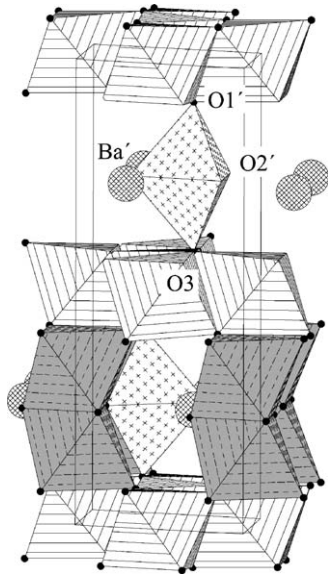

Fig. 4. Projection of the structure of BaV_6O_{11} at 293 K; for reasons of clearness the structure is slightly rotated out of the ideal b,c-projection; octahedra around V(1) and trigonal bipyramids around V(3) are indicated; $V(2)O_6$-octahedra are only shown in the lower part; large hatched circles represent Ba-atoms; drawn with Atoms [29].

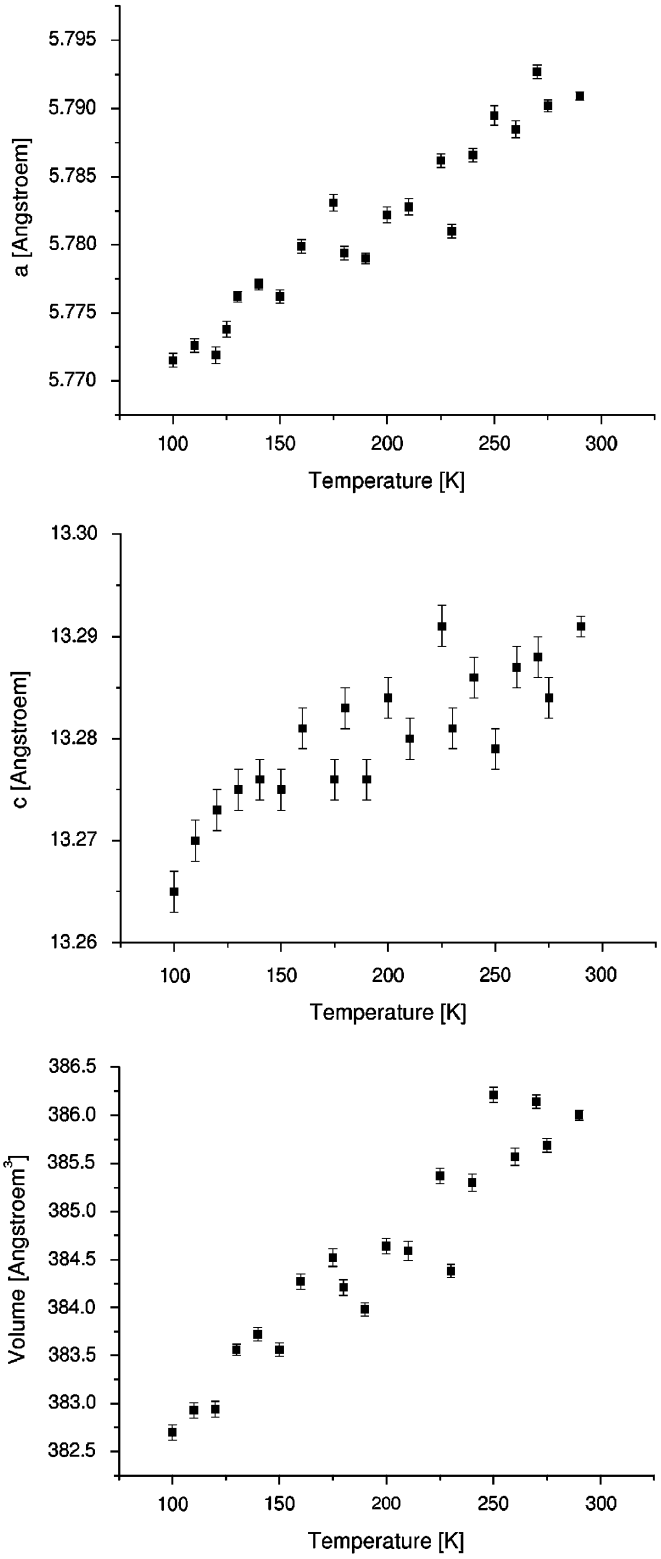

Fig. 5. Temperature dependence of lattice parameters in (Å) and unit cell volume in [Å^3].

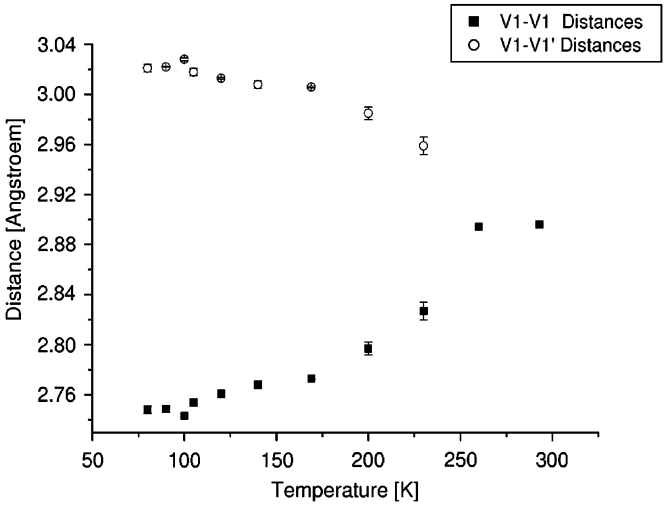

Fig. 6. V1–V1-distances in BaV_6O_{11} as a function of temperature.

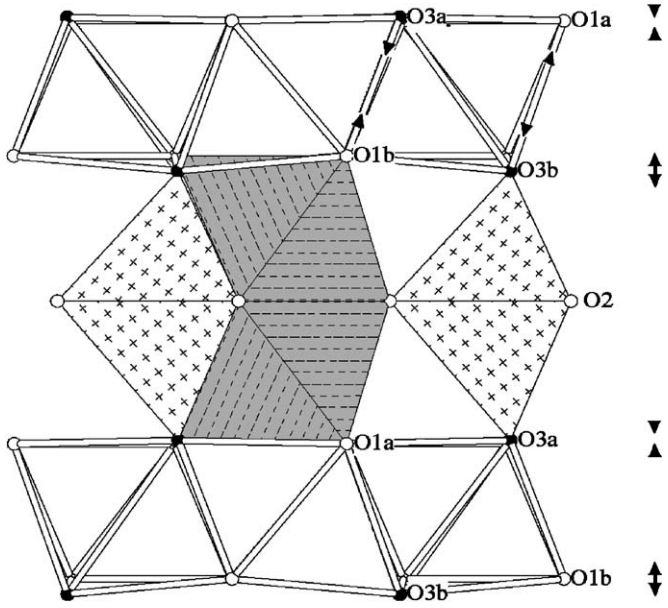

Fig. 7. Partial view of the structure of BaV_6O_{11} at 80 K; the movements of the O(1a)/O(1b) and O(3a)/O(3b) atoms with respect to the high-symmetry structure are indicated. Octahedra around V(1) and V(2a)/V(2b) and trigonal bipyramids V(3) are shown; drawn with Atoms [29].

atoms of the sheet, namely O(1)/O(3) or O(1a)/O(3a) and O(1b)/O(3b), respectively, show no significant change of their x and y coordinates at any of the temperatures. Yet their z coordinates behave in a striking way: while in the centrosymmetric structure both bottom and top of the layer are slightly corrugated, in the low-temperature phase one side of the layer is clearly more corrugated while the other tends to become even when the temperature is lowered further (see Fig. 7).

This change is best quantified by the differences of the z coordinates of the limiting oxygen atoms in both phases (see Fig. 8). The difference for the pair of atoms O(1a)–O(3a) decreases, while the difference between the coordinates of O(1b) and O(3b) increases down to the

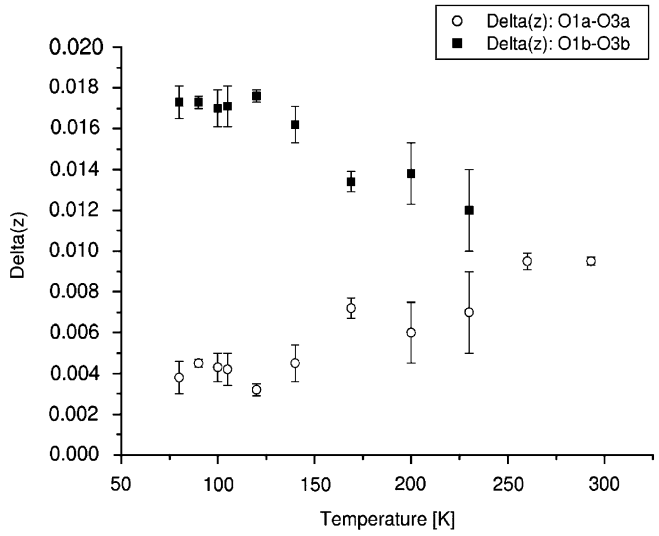

Fig. 8. Differences in the z-coordinates of the O atoms limiting the octahedral sheet.

temperature of the magnetic transition (115 K) and afterwards seems to maintain itself at a constant value.

Apart from the changes associated to the structural transition at 250 K, an analysis of the temperature dependence of the geometrical characteristics in the structure is best described by analyzing the cation coordination polyhedra:

- The change in the unit cell volume corresponds to a decrease in the volume of the $[BaO_{12}]$-coordination polyhedra. Within the Ba–O polyhedra the Ba–O(1a) distances increase slightly, the Ba–O(1b) distances decrease. Ba–O(2) distances remain basically constant over the whole temperature range.
- The volume of the $[V(1)O_6]$-octahedra in the octahedral sheet remains constant, though, due to the fact that the V(1)–O(1a) and V(1)–O(3b) distances decrease, while at the same time the V(1)–O(1b) and V(1)–O(3a) distances increase with lower temperatures (see Fig. 9, top), the overall deformation of the octahedra is considerably increased. A tendency to keep the V(1)–O distances constant once the temperature of the magnetic anomaly at 115 K is reached can be observed.

  O–O distances in the plane perpendicular to the c-axis show no significant temperature dependency. Of the distances determining the thickness of the octahedral layer, the O(1a)–O(1b) distance remains also constant over the whole temperature range. However, the O(1a)–O(3b) and O(1b)–O(3a) distances change rather drastically, the first one increasing with decreasing temperature, the second one decreasing (see Fig. 9, middle). This change in distances is also reflected in the changes of the corresponding inter-octahedral angles: the O(1a)–V(1)–O(3b) angle drastically increases while at the same time the opposing O(1b)–V(1)–O(3a) angle decreases (see Fig. 9, bottom). Both angles describing

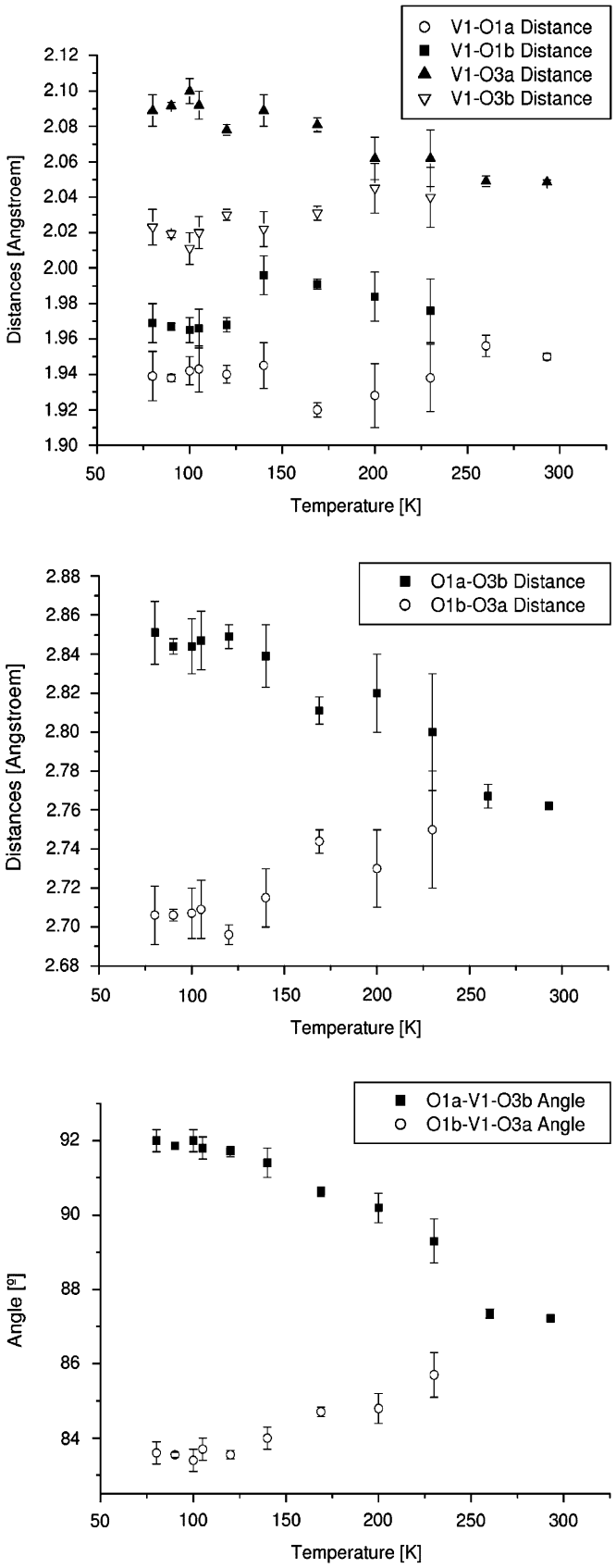

Fig. 9. Geometrical changes in the $V(1)O_6$ coordination polyhedra as a function of temperature. Top: V(1)–O distances; middle: O1a–O3b and O1b–O3a octahedral edge lengths; bottom: O1a–V(1)–O3b and O1b–V(1)–O3a angles.

the axis of the octahedra, O(1a)–V(1)–O(1b) and O(3a)–V(1)–O(3b) reach values significantly smaller than the ideal value of 180°. In comparison changes of the other angles in the octahedra are small.

- Of the two face sharing [V(2)O_6]-octahedra one decreases significantly in volume ([V(2a)O_6]), while the other one increases slightly ([V(2b)O_6]). The V2–V2 (or V2a–V2b, respectively) distances do not change significantly in the temperature range studied.
  Changes of V(2)–O distances are small and hardly significant (see Fig. 10, top). While O(2)–O(2) distances keep constant over the whole temperature range, the O(1a)–O(2) and O(1b)–O(2) distances decrease or increase, respectively. The above described volume changes of the [V(2)O_6]-octahedra is mainly ascribed to small but significant changes of the O(1a)–O(2)/O(1b)–O(2)-distances coupled with the corresponding modifications in the O–V(2)–O angles.
- The volume of the [V(3)O_5]-bipyramid is decreased. This can be mainly attributed to the shift of the O(3a) and O(3b) atoms, as the short equatorial V(3)–O(2) distances keep constant over the full temperature range. For both distances V(3)–O(3a) and V(3)–O(3b) a small discontinuity at the temperature of the magnetic transition at 115 K may be assumed (see Fig. 10, bottom). The increase in the O(2)–O(3a) distance and the corresponding angle O(2)–V(3)–O(3a) and the decrease in the O(2)–O(3b) distance and O(2)–V(3)–O(3b)-angle, respectively, lead to a deformation of the bipyramid. Due to this deformation the volumes of the two halves of the bipyramid become clearly unequal.

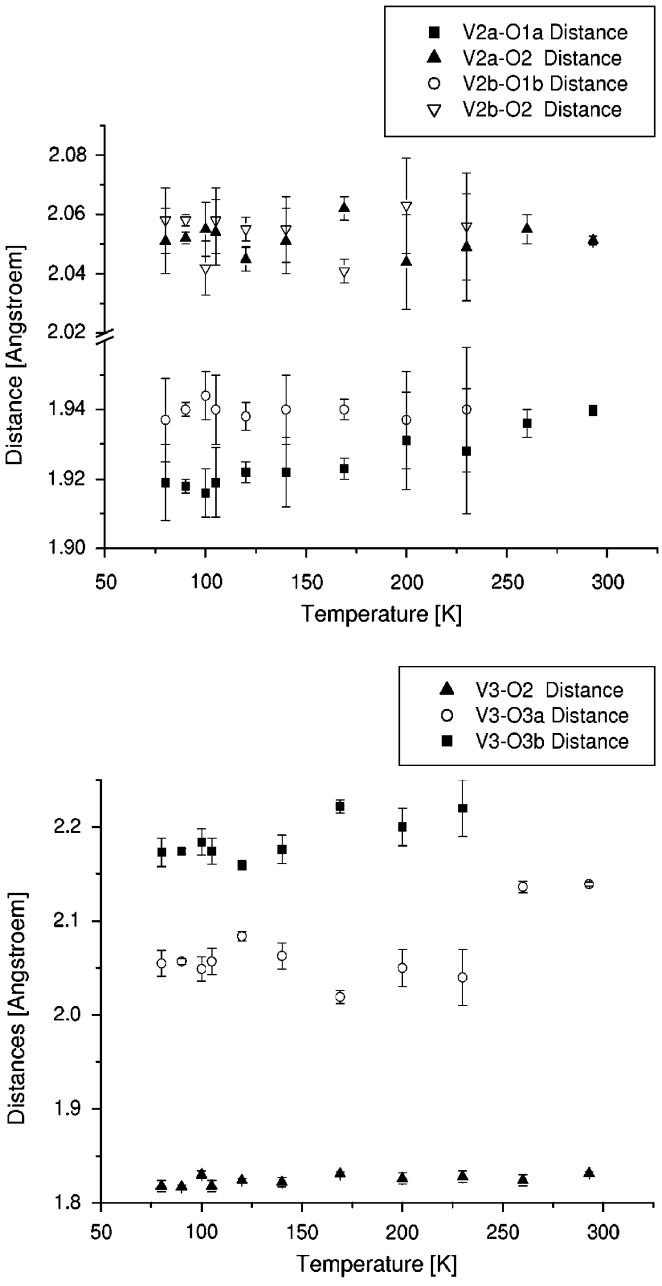

Fig. 10. V(2)–O and V(3)–O distances in BaV_6O_{11} as a function of temperature.

As a summary, we can say that the structural phase transition at approximately 250 K is characterized by a small displacement of the V(1)-atom out of its central position in the octahedra. This movement leads to a deformation of the octahedra, where part of the octahedral edges/angles are increased, while the opposite ones are decreased. As a consequence one limiting surface of the octahedral sheet is corrugated, while the other one is smoothened with respect to the high-temperature structure. This deformation of the octahedral sheets leads to the corresponding geometrical changes in the other coordination polyhedra.

Response of the structure to the magnetic transition at 115 K is weak and mainly observable in the geometric parameters concerning the [V(1)O_6]-octahedra and [V(3)O_5]-bipyramids. This may serve as a first indication that the corresponding central atoms play an important role in the mechanism of the magnetic phase transition, yet more detailed investigation on the magnetic characteristics of this compounds are indispensable to draw any definite conclusions.

Acknowledgments

We thank Andrzej Grzechnik for his collaboration regarding the determination of lattice parameters. We are grateful to M. Akaishi for support with high-pressure experiments. K.F. acknowledges financial support by the Science and Technology Agency of Japan and the Spanish 'Ministerio de Educación y Cultura'. We acknowledge the ANKA Angstroemquelle Karlsruhe for the provision of beamtime and would like to thank Dr. G. Buth for assistance using the beamline SCD.

References

[1] M.E. de Roy, J.P. Besse, R. Chevalier, M. Gasperin, J. Solid State Chem. 67 (1987) 185–189.

[2] Y. Kanke, F. Izumi, E. Takayama-Muromachi, K. Kato, T. Kamiyama, H. Asano, J. Solid State Chem. 92 (1991) 261–272.
[3] O. Mentre, F. Abraham, J. Solid State Chem. 125 (1996) 91–101.
[4] Y. Kanke, Phys. Rev. B 60 (1999) 3764–3776.
[5] Y. Kanke, E. Takayama-Muromachi, K. Kato, Y. Matsui, J. Solid State Chem. 89 (1990) 130–137.
[6] Y. Uchida, Y. Kanke, E. Takaya-Muromachi, K. Kato, J. Phys. Soc. Japan 60 (1991) 2530–2533.
[7] Y. Kanke, K. Kato, E. Takayama-Muromachi, M. Isobe, Acta Crystallogr. C 48 (1992) 1376–1380.
[8] Y. Kanke, F. Izumi, Y. Morii, E. Akiba, S. Funahashi, K. Kato, M. Isobe, E. Takayama-Muromachi, Y. Uchida, J. Solid State Chem. 112 (1994) 429–437.
[9] Y. Kanke, H. Shigematsu, K. Ohshima, K. Kato, J. Appl. Crystallogr. 28 (1995) 599–603.
[10] Y. Uchida, Y. Kanke, J.S. Lord, P.C. Riedi, J. Magn. Magn. Mater. 140 (1995) 163–164.
[11] D.K. Seo, M.H. Whangbo, J. Am. Chem. Soc. 118 (1996) 3951–3958.
[12] O. Mentre, A.C. Dhaussy, F. Abraham, H. Steinfink, J. Solid State Chem. 130 (1997) 223–233.
[13] M. Iwata, Y. Ishibashi, J. Phys. Soc. Japan 67 (1998) 691–692.
[14] A. Akiba, H. Yamada, R. Matsuo, Y. Kanke, T. Haeiwa, E. Kita, J. Phys. Soc. Japan 67 (1998) 1303–1305.
[15] Y. Hata, Y. Kanke, E. Kita, H. Suzuki, G. Kido, J. Appl. Phys. 85 (1999) 4768–4770.
[16] E. Goering, D. Ahlers, K. Attenkofer, G. Obermeier, S. Horn, G. Schutz, J. Synchrotron Rad. 6 (1999) 537–539.
[17] A.-C. Dhaussy, O. Mentre, F. Abraham, Y. Calage, J. Solid State Chem. 147 (1999) 609–617.
[18] H. Kato, M. Kato, K. Yoshimura, K. Kosuge, J. Phys. Soc. Japan 70 (2001) 1404–1410.
[19] Y. Uchida, M. Onoda, Y. Kanke, J. Magn. Magn. Mater. 226 (2001) 446–448.
[20] H. Kato, M. Kato, K. Yoshimura, K. Kosuge, J. Phys. Condens. Matter 13 (2001) 9311–9333.
[21] O. Mentre, Y. Kanke, A.-C. Dhaussy, P. Conflant, Y. Hata, E. Kita, Phys. Rev. 64 (2001) 174404.
[22] S.H. Kilcoyne, Physica B 326 (2003) 532–535.
[23] A. Villesuzanne, M.-H. Whangbo, H.-J. Koo, Chem. Mater. 17 (2005) 4344–4349.
[24] S. Ishiwata, D. Wang, T. Saito, M. Takano, Chem. Mater. 17 (2005) 2789–2791.
[25] M.L. Foo, Q. Huang, J.W. Lynn, W.-L. Lee, T. Klimczuk, I.S. Hagemann, N.P. Ong, R.J. Cava, J. Solid State Chem. 179 (2006) 563–572.
[26] STOE & CIE GmbH, X-AREA: STOE IPDS Software, Version 2.87, Computer Program, Darmstadt, Germany, 1998.
[27] V. Petříček, M. Dušek, L. Palatinus, JANA2000-Crystallographic Computing System, Institute of Physics, Academy of the Czech Republic, Praha, 2000.
[28] A. Altomare, G. Cascarano, C. Giacovazzo, A. Guagliardi, A.G.G. Moliterni, M.C. Burla, G. Polidori, M. Camilli, R. Spagna, SIR97—a Package for Crystal Structure Solution by Direct Methods and Refinement, Computer Program, Dip. Geomineralogico, University of Bari, Italy, 1997.
[29] E. Dowty, Atoms Version 5.0.7, Computer Program, 1997.